Global Ecology and Conservation 19 (2019) e00683

Contents lists available at ScienceDirect

Global Ecology and Conservation

journal homepage: http://www.elsevier.com/locate/gecco

Review Paper

Passive remote sensing technology for mapping bull kelp (*Nereocystis luetkeana):* A review of techniques and regional case study

Sarah B. Schroeder [a, *], Colleen Dupont [a], Leanna Boyer [b], Francis Juanes [c], Maycira Costa [a]

[a] Spectral Lab, University of Victoria, Victoria, B.C, V8P 5C2, Canada
[b] SeaChange Marine Conservation Society, Brentwood Bay, B.C, V8M 1R3, Canada
[c] Department of Biology, University of Victoria, Victoria, B.C., V8P 5C2, Canada

ARTICLE INFO

Article history:
Received 31 January 2019
Received in revised form 4 June 2019
Accepted 4 June 2019

Keywords:
Kelp
Remote sensing
Habitat mapping
Macro algae
Digital image processing
Review

ABSTRACT

The distribution and abundance of the canopy-forming kelp *Nereocystis luetkeana* is of increasing concern for environmental management and conservation in coastal regions due to its importance as a foundation species. Mapping kelp forests aids in understanding their health, productivity, and response to environmental conditions. Remote sensing using satellites is an increasingly accessible tool for mapping nearshore habitats allowing for applications such as long-term monitoring and large- and small-scale surveys. This paper provides a review of passive optical remote sensing techniques for detection and mapping of floating macro-algae, and adapts these techniques for detecting *Nereocystis luetkeana*, demonstrating their application through a comprehensive case study, from imagery acquisition to map validation. This review with associated case study communicates to non-remote sensing experts a road map to use remote sensing technology for mapping kelp habitats.

1. Introduction

Bull kelp *(Nereocystis luetkeana)* is a brown algae in the order Laminariales, and represents one of two important canopy-forming kelp species found in marine nearshore habitats on the west coast of North America, along with giant kelp (*Macrocystis pyrifera*) (Druehl, 1970). Although the two species have similar ranges, extending from Alaska to California, there are differences in local scale distribution due to variations in tolerance to temperature and wave exposure. Often referred to as a foundation species, beds of bull kelp form structural underwater forests that offer habitat for fish and invertebrates (Christie et al., 2009; Trebilco et al., 2015), and provide nutrients to grazers and to detrital food webs as wrack (Dugan et al., 2011; Duggins et al., 2001). Also, the three-dimensional structure of beds acts as a physical barrier, reducing coastal erosion and dampening wave action (Duggins, 1988; Eckman et al., 1989). The importance of this species in nearshore ecosystems makes its abundance and distribution of great concern to environmental monitoring and management (Krumhansl et al., 2016; Mumford, 2007; Springer et al., 2007; Teagle et al., 2017).

* Corresponding author.
E-mail address: sbs@uvic.ca (S.B. Schroeder).

https://doi.org/10.1016/j.gecco.2019.e00683

Several factors determine bull kelp distribution and abundance. Natural factors include grazing pressure (Taylor et al., 2018), physical disturbance from wave action (Reed et al., 2011), and natural variations of light availability, nutrients, and temperature (Bell et al., 2015a; Pfister et al., 2017). Anthropogenic factors include direct harvest (Sutherland et al., 2008), increase in herbivores through removal of predators by fisheries (Halpern et al., 2006; Ling et al., 2009), coastal pollution through wastewater (Foster and Schiel, 2010), increased turbidity from shoreline development (Deiman et al., 2012; Dethier et al., 2016), as well as climate change-induced sea temperature change, ocean acidification, and increased storm activity (Byrnes et al., 2011; Hernández et al., 2018; Vergés et al., 2016). For instance, there have been reports of bull kelp decline following abnormally high temperature disturbances and local scale losses attributed to regions with high anthropogenic stress (Pfister et al., 2017; Schiel et al., 2004). In many regions, however, data on the spatial temporal distribution and abundance of bull kelp are lacking, making it difficult to define the impact of human activities and environmental drivers on this ecologically important foundation species.

Remote sensing technology, including aerial, drone, and satellite imagery, is becoming a key component of kelp monitoring programs (Cavanaugh et al., 2010; Bell et al., 2015b; Casal et al., 2013; Pfister et al., 2017). Specifically, satellite data is advantageous for mapping large areas as it provides multi-temporal data in both visible and infrared wavelengths, and requires less time and labour than traditional boat- or diver-based surveys (Casal et al., 2011). Furthermore, remote sensing technologies have the potential to improve spatial and temporal coverage through automation and repeatability (Augenstein et al., 1991; Nijland et al., 2019). Through the use of remote sensing technology, we now have a better understanding of regional kelp community dynamics, temporal trends, and oceanographic effects in these communities (Bell et al., 2015a; Cavanaugh et al., 2011).

There is a growing body of research using remote sensing for detecting several species of floating algae, including giant kelp (Augenstein et al., 1991; Bell et al., 2015b; Cavanaugh et al., 2011, 2010; Deysher, 1993; Donnellan and Foster, 1999; Fyfe et al., 1999; Kim et al., 2010), *Sargassum* (Dierssen et al., 2015; Gower et al., 2006; Gower and King, 2008; Marmorino et al., 2011; Wang and Hu, 2016), and green algae (Cui et al., 2012; Keesing et al., 2011; Ma et al., 2009; Shi and Wang, 2009). In comparison, relatively few studies have used satellite remote sensing to map bull kelp due to the challenge of detecting the generally smaller beds found in close proximity to rocky shorelines (Stekoll et al., 2006). Although key differences exist between various species of floating macro algae, the general principles for detection with remote sensing are similar. Therefore, the methods for detecting giant kelp, green algae, and *Sargassum* are a foundation for developing methods for remote sensing of bull kelp. The objectives of this paper are to (1) outline the principles for optical remote sensing of bull kelp, (2) review methods used by studies to map macro algae and their relevance to bull kelp mapping, and (3) illustrate a methodology for optical remote sensing of bull kelp with a case study in British Columbia, Canada.

2. Optical remote sensing of bull kelp: principles

The principles for optical remote sensing of bull kelp are based on the algae's morphology and growth patterns, along with the spectral properties of the algae, surrounding seawater, and its optical constituents.

2.1. Optical properties of kelp beds

Bull kelp beds are composed of many kelp sporophytes, which grow at or near the water's surface; they may form a dense or sparse canopy, depending on the number and proximity of individuals. The reflectance from kelp beds is composed of signals from the kelp plants floating on the water's surface, as well as water and its optical constituents. As Fig. 1 shows, the above-water reflectance signal corresponding to different densities of kelp is generally most prominent at the visible (VIS) and near infrared (NIR) spectra, similar to vascular plants (Cavanaugh et al., 2010; Jensen et al., 1980), and is a result of its physiological and morphological characteristics.

Kelp reflectance at visible wavelengths is largely due to the photosynthetic pigments chlorophyll-a, chlorophyll-c, and fucoxanthin present in the chloroplasts (Wheeler et al., 1984). Dominant pigments are chlorophyll-a with peak absorption at 435 and 675 nm, chlorophyll-c with peak absorption around 460 and 633 nm, and fucoxanthin, absorbing between 500 and 550 nm (Anderson et al., 1979; Kotta et al., 2014). The absorption characteristics of these pigments result in the brownish colour of the kelp (Charrier et al., 2012); note in Fig. 1 the lower reflectance in the blue and green wavelengths due to the higher absorption by pigments and slightly higher reflectance towards the red wavelengths. Higher reflectance in the near infrared spectra between 700 and 900 nm is mostly due to the internal cellular structure of the central tissues, which refract and strongly reflect these longer wavelengths (Liew et al., 2008). Pure water, on the other hand, is characterized by low reflectance across all wavelengths and very high absorption in the near infrared due to the absorption properties of water molecules (Mobley, 1994).

When kelp beds are sparse or partially submerged, the detected near infrared reflectance is a combination of the high signal from kelp and low signal from the highly absorbing surrounding water. This reduces the overall signal of both the red and infrared wavelengths (see sparse and submerged kelp vs dense kelp spectral signatures in Fig. 1). Furthermore, optical constituents present in the seawater can reduce contrast between the beds and surrounding water, decreasing the detectability of kelp beds. For example, phytoplankton may form dense blooms and increase the near infrared reflectance of seawater (Babin et al., 2003), and suspended sediments generally increase visible and near infrared reflectance, especially red

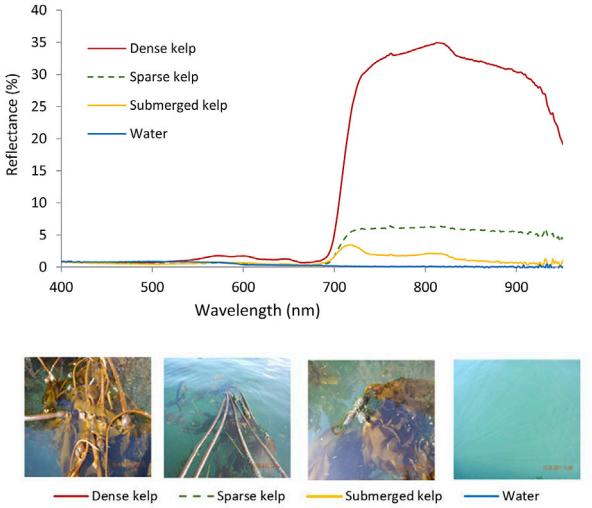

Fig. 1. Reflectance of dense (>50% of 1 m^2 covered), sparse (<50% of 1 m^2 covered), submerged kelp (all plants slightly below water surface) and ocean water measured with a Fieldspec Pro® spectroradiometer in the coastal waters of British Columbia, Canada.

wavelengths (Roesler and Perry, 1995). Coloured dissolved organic matter (CDOM) strongly absorbs visible light, resulting in decreased reflectance in blue wavelengths (Brezonik et al., 2015).

2.2. Bull kelp morphology and growth

Growth of the bull kelp sporophytes begins in early spring, after which plants grow rapidly and can reach sizes greater than 10 m in height at their maximum extent by late summer. The physical condition of the sporophyte deteriorates due to prolonged exposure to high currents and temperatures, resulting in dislocation and removal of the plant by fall and winter (Mumford, 2007). Because of its annual growth cycle, late summer is generally the best period for mapping bull kelp.

Each kelp plant is composed of a root-like holdfast that anchors to hard rocky substrate, a long, hollow stem-like stipe, and an air-filled bulb called a pneumatocyst up to 15 cm in diameter (Amsler and Neushul, 1989) from which multiple blades or lamina grow (Fig. 2b). The buoyancy of the bulb and stipe allow the plant to stand upright in the water column and the blades to form a canopy. The portion of kelp canopy floating on the surface or just below the surface allows remote sensing platforms to detect the macro algae (Fig. 2a). However, the proportion of kelp canopy at the water's surface can change depending on the length of the kelp, tidal height, currents, bathymetry, and water conditions (Fig. 2b).

The density of kelp canopy at the surface will also affect the reflectance detected by a sensor and its ability to discriminate kelp from water. While there is no standard measure to define dense or sparse beds, the distinction may be based on the objective of the study. Aerial-based methods such as Kelp Inventory Monitoring (KIM-1) and its modifications used in British Columbia to quantify kelp extent and biomass (Foreman, 1975; Sutherland et al., 2008) calculate *Nereocystis* density directly from imagery using a point intercept method, and define dense beds as greater than 10 plants per 10 square metres, and sparse as fewer than 10 plants. Other methods have defined density by the percent coverage of plants or fronds visible at the surface, where low density is less than 15% and high density is greater than 15% of a given area (Sutherland et al., 2008). These methods are well suited to remote sensing-based detection where only the reflectance of surface plants can be detected.

3. Methods for optical remote sensing of macro algae

We compiled a literature review of studies on the subject of remote sensing of macro algae species including *Nereocystis luetkeana*, *Macrocystis pyrifera*, canopy-forming Laminariales, and other species of floating macro algae, aiming to summarize the methods applicable to the detection of bull kelp. Although the reviewed methods focus on various macro algae species such as *Ulva*, *Sargassum*, and *Macrocystis*, which all have differences in their morphological, temporal, spatial, and spectral characteristics, the remote sensing-based mapping protocols follow the same basic steps and techniques (workflow illustrated in Fig. 3).

3.1. Imagery acquisition

One of the first steps in remote sensing-based mapping projects is imagery acquisition. The optimal sensor to employ depends on the relationship between the spectral, spatial, and temporal characteristics of the target species and the sensor. Aerial cameras (Donnellan and Foster, 1999; Fyfe et al., 1999; Hu et al., 2015; Nezlin et al., 2007), airborne hyperspectral (Hu

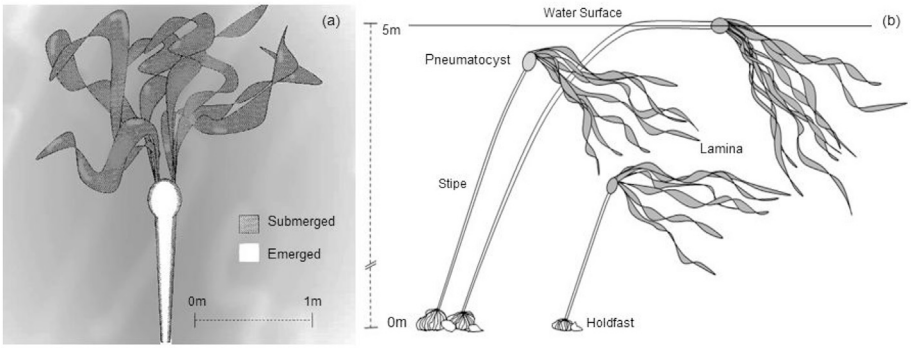

Fig. 2. (a) Overhead view (satellite view) of floating bull kelp, with the bulb and part of the stipe emerged, and the blades submerged in water. (b) Bull kelp bed cross-section. The length of the stipe and the height of the tide affects whether kelp is submerged or emerged.

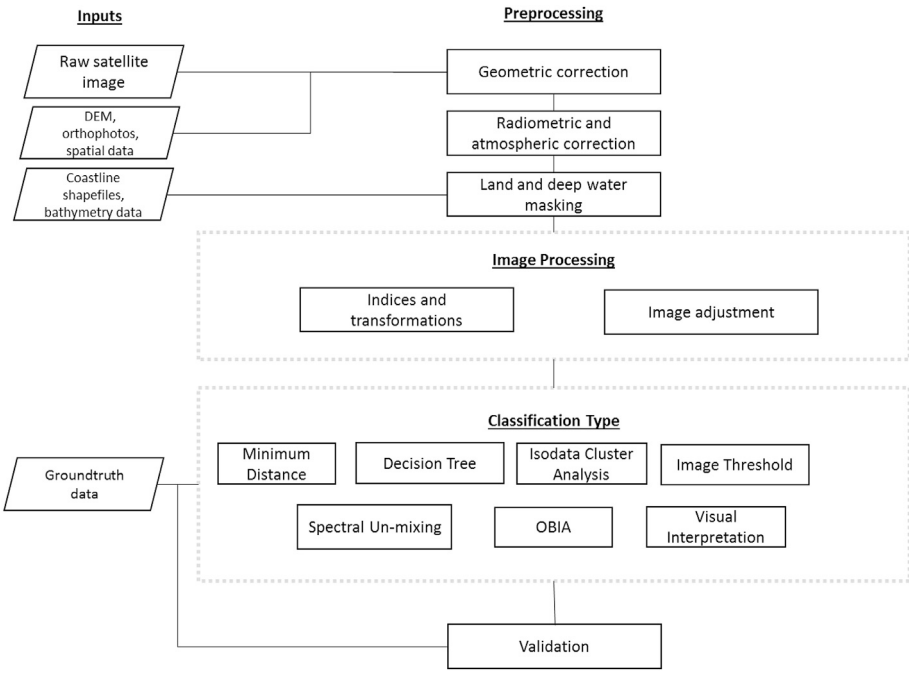

Fig. 3. Generalized workflow for mapping floating macro algae with optical imagery, following previous research.

et al., 2015; Stekoll et al., 2006) and multispectral imaging systems (Stekoll et al., 2006), space-borne multispectral sensors (Casal et al., 2011; Cavanaugh et al., 2010; Garcia et al., 2013; Gower and King, 2008; Hu, 2009; Kim et al., 2010), and more recently, unmanned aerial vehicles (Duffy et al., 2018) have been used in macro algae detection. Along with choosing an appropriate sensor, timing of imagery acquisition is crucial for successful mapping of macro algae. While some macro algae, such as pelagic *Sargassum* and *Ulva*, float freely on the surface and are therefore not affected by tidal height, other macro algae, such as bull kelp, is most exposed during low tide and weak currents, thus defining optimal conditions for imagery acquisition. Furthermore, cloud cover, water roughness, sun angle, and water column constituents also affect the visibility of macro algae. Rough waters, such as those with breaking waves, can obscure the reflectance of the underlying kelp. Waves and ripples alter the angle between incoming solar radiation and the surface of the water, causing glint, which results in high reflectance across visible and NIR wavelengths and may obscure kelp (Hedley et al., 2005). In practice, it is difficult to time surveys and conditions perfectly; consequently, data are often acquired under sub-optimal circumstances (Casal et al., 2011; Kay et al., 2009).

3.1.1. Aerial sensors

Aerial imagery utilizes sensors fixed on aircraft to collect overlapping images covering the study area. Images are then used to create orthophotos for delineating kelp beds and deriving products. RGB cameras, near infrared, or hyperspectral sensors

may be used depending on the objectives of the project. Near infrared (NIR) aerial imagery has been used since the 1930s for mapping kelp resources, for instance, in California for monitoring giant kelp (Deysher, 1993; North et al., 1993), in British Columbia to inventory kelp resources (Foreman, 1975; Sutherland et al., 2008), and in Washington State to map kelp aerial extent, species, and density (Pfister et al., 2017; Van Wagenen, 2015). Beyond NIR imagery, airborne hyperspectral imagers such as AVIRIS, CASI, AISA, and PRISM collect spectral information in very narrow bands over many wavelengths, and provide both high spatial and spectral resolutions, which is beneficial in discriminating between similar species (Dierssen et al., 2015; O'Neill and Costa, 2013). A major benefit of aerial sensors on aircraft is the control of survey timing, temporal, and spatial resolutions so that data acquisition can be optimized, however the costs can be high (Anderson et al., 2007). There are private companies that can be contracted to fly and collect images, some of which may process the data into orthophotos for use in classification.

3.1.2. Unmanned aerial vehicles (UAV)

The use of unmanned aerial vehicles or drones is becoming increasingly common for all types of habitat mapping (Duffy et al., 2018; Hardin and Jensen, 2011; Kislik et al., 2018; Murfitt et al., 2017; Nahirnick et al., 2018; Nahirnick et al., 2018). This method is the most flexible in terms of controlling for environmental variables and flight times; however, it is limited to small areas of spatial coverage. Depending on the altitude of data collection, imagery resolution can be extremely high (<1 cm) (Murfitt et al., 2017), allowing visual counts of individual plants and discrimination of species (Murfitt et al., 2017; Nahirnick et al., 2018). Site-specific studies aiming to estimate parameters such as kelp biomass may be well served by this method. Costs will include the purchase of an appropriate UAV able to carry the sensor of choice (RGB cameras such as a GoPro® or higher-end NIR, multispectral and hyperspectral) and GPS; further requirements are related to country-dependent license and air space limitations. Alternatively, several UAV-based contracting companies are available. In order to accurately process the images, users will need access to appropriate software to create orthomosaics and georeference the images for use in classification (see Kislik et al., 2018).

3.1.3. Satellite sensors

Spaceborne multispectral imagers are a feasible choice for detecting floating macro algae due to their relatively low cost, high spatial coverage, and available archived data. The various satellite sensors used in previous research (Tables 1 and 2) have differing specifications, and therefore different applications for macro algae detection. Coarse spatial resolution imagery from MODIS (250–1000 m) has been used to create indices for large floating macro algae blooms such as *Sargassum* and *Ulva* in the open ocean (Cui et al., 2012; Garcia et al., 2013; Gower et al., 2006; Gower and King, 2008; Hu, 2009; Hu et al., 2015; Keesing et al., 2011; Shi and Wang, 2009). Medium spatial resolution data from sensors such as Landsat (30 m) and SPOT (6 m) have been used for detecting giant kelp (Bell et al., 2015b; Casal et al., 2011; Cavanaugh et al., 2011, 2010; Deysher, 1993). On the other hand, mapping of nearshore, fringing bull kelp beds requires sensors with metre to sub-metre spatial resolution, such as the QuickBird and WorldView series. Hyperspectral sensors are being planned for the future, and will provide high spectral resolution imagery, which may be necessary to differentiate among species, but have coarser spatial (60 m) and temporal resolutions (Bell et al., 2015b). A proof of concept was the HICO sensor onboard the International Space Station, which has proven to be effective for differentiating *Sargassum* from garbage, oil, and other algae (Hu et al., 2015).

There are various procedures for acquiring satellite imagery depending on whether it is freely available or provided by proprietary satellites. Free imagery, such as the Landsat series and Sentinel, can be downloaded from the United States Geological Survey (USGS) and European Space Agency (ESA) (https://earthexplorer.usgs.gov/). Several generations of Landsat satellites have been in operation from 1972 to the present, and while older sensors had lower spatial resolution and differing spectral bands, the data is a valuable resource and has been utilized by numerous macro algal studies to understand drivers of change over long time periods (Anderson et al., 2007; Bell et al., 2018; Nijland et al., 2019). MODIS and MERIS are also freely available; images cover large areas (185-100 km) but with coarse spatial resolution (≥250 m). Higher spatial resolution satellites such as the WorldView Series, GeoEye, and QuickBird are proprietary, and imagery can be bought from archived databases or tasked for a specific time and location. The cost of a tasked mission is typically a few thousand dollars ($27–45 USD per km^2) as there is a minimum order size required.

3.2. Ground-truthing data

For floating macro algae studies, field observations are required to validate remote sensing classifications (Richards and Congalton, 2001), to train supervised classifications (Casal et al., 2011), and to inform product creation such as biomass estimates (Cavanaugh et al., 2010; Stekoll et al., 2006). Ground-truth surveys of kelp are often undertaken by boat, and may involve using divers if biological parameters such as lengths and weights are needed (Stekoll et al., 2006). Basic requirements for ground-truth data are an accurate record of where kelp is located in at least a subset of the area to be imaged. Additional data collected can help with understanding variability within a scene and may include: other species present; physical conditions such as wind speed, surface conditions, tide height, depth of kelp, Secchi depth, or water turbidity; and bed density estimates. More detailed data such as individual plant location, length, and wet/dry weights may also be recorded if products such as biomass are being derived from imagery. For biomass estimates, the location and number of sampling sites may also have an effect on results. For instance, plots placed in the center of beds may be more representative of site-wide biomass than those at the edges (Cavanaugh et al., 2010). A key consideration for field surveying is to acquire field data concurrently

Table 1
Remote sensing of floating macro algae studies relevant to the detection of bull kelp. Note that this table is not a comprehensive list of all studies, but presents a sample of relevant techniques from the literature.

Species	Sensor(s)	Image Processing	Classification	Study
Ecklonia maxima, Laminaria pallida	Colour infrared aerial photography, Landsat 7, Landsat 5	Bispectral and principal component (PC) analysis	Spectral Angle Mapper, supervised classification	Anderson et al. (2007)
Macrocystis pyrifera	HyspIRI, Landsat 5, AVIRIS	MESMA: multiple endmember spectral mixing analysis	MESMA threshold	Bell et al. (2015b)
Laminariales spp.	SPOT 4	Histogram equalization, band ratios	Supervised angular, unsupervised cluster, visual	Casal et al. (2011)
Macrocystis pyrifera	SPOT 5	NDVI, PC analysis	NDVI threshold	Cavanaugh et al. (2010)
Macrocystis pyrifera	Landsat 5	MESMA	MESMA threshold	Cavanaugh et al. (2011)
Macrocystis pyrifera	SPOT 1, 2	NIR:RED ratio	Density thresholds	Augenstein et al. (1991)
Enteromorpha prolifera	HJ-1 A/B, ASAR, MODIS	NDVI backscattering interpretation	NDVI threshold	Cui et al. (2012)
Macrocystis pyrifera	SPOT 1, ADAR	Histogram normalization, contrast enhancement, band ratios	Unsupervised cluster, CLUST analysis	Deysher (1993)
Macrocystis pyrifera	Colour infrared aerial photography	N/A	Visual interpretation	Donnellan and Foster (1999)
Sargassum spp., *Syringodium filiform*	PRISM	Spectral resampling, NDVI	Custom stepwise classification	Dierssen et al. (2015)
Zostera noltii	Colour aerial photography (UAV)	RGB and texture of green band	Unsupervised and OBIA	Duffy et al. (2018)
Macrocystis pyrifera	Colour aerial photography	N/A	Unsupervised classification	Fyfe et al. (1999)
Enteromorpha prolifera	MODIS	Modified SAI on NDVI	SAI threshold	Garcia et al. (2013)
Sargassum spp.	MERIS, MODIS	MCI, FLH	Visual interpretation	Gower et al. (2006)
Enteromorpha prolifera	MODIS, Landsat	FAI	FAI threshold	Hu (2009)
Sargassum spp.	MODIS, Landsat, WorldView-2, HICO, AVIRIS, airborne digital photos	FAI, NDVI, MCI, SI, LD	Stepwise classification including index thresholds	Hu et al. (2015)
Macrocystis pyrifera	Landsat, colour infrared aerial photography, radar	Near Infrared Band	Supervised Classification	Jensen et al. (1980)
Enteromorpha prolifera	MODIS	SAI: scaled algae index	SAI threshold	Keesing et al. (2011)
Macrocystis pyrifera	QuickBird	NDVI, panchromatic band	Brightness threshold	(Kim et al., 2010)
Enteromorpha prolifera	MODIS	Ratio bands 1 and 2, analysis of chlorophyll-a product	Index threshold	Ma et al. (2009)
Sargassum spp.	CASI, thermal infrared imagery	Spectral and thermal interpretation, red-edge calculation	Red-edge threshold	Marmorino et al. (2011)
Macrocystis pyrifera, Nereocystis luetkeana	Colour infrared aerial photography	Near infrared reflectance, contrast enhancement	Visual interpretation	Pfister et al. (2017)
Enteromorpha prolifera	MODIS	NDAI (normalized difference algae index)	NDAI threshold	Shi and Wang (2009)
Nereocystis luetkeana, Alaria fistulosa	Colour infrared aerial photography	Log transformed, normalized difference using blue and NIR bands	ISODATA unsupervised classification	Stekoll et al. (2006)
Laminaria digitata, Saccharina latissima	Custom airborne hyperspectral imager	N/A	Bayesian supervised classification, differential histogram equalization	Volent et al. (2007)

with imagery acquisition. However, it is often difficult to achieve simultaneous collection, so the time between acquisitions should be minimized and considered during image processing and interpretation (McCoy, 2005).

Although collecting field data is important for training and for validating a model for classification, it is not always feasible due to inaccessibility of a study area or when using historical imagery. Alternatively, some studies use data from historical maps, classified aerial photography, and algae harvesting records (Casal et al., 2011; Cavanaugh et al., 2010; Deysher, 1993; Donnellan and Foster, 1999). In some cases, such as the pelagic *Sargassum* survey by Marmorino et al. (2011), alternatives for field data were not available and accuracy assessment was omitted. Similarly, several studies of the *Ulva* bloom in the Yellow Sea proceeded without field data (Keesing et al., 2011; Ma et al., 2009), however, local knowledge was used as the bloom was

Table 2
Remote sensors used for floating macro algae detection.

Sensor	Spatial Resolution (m)	Spectral Range (nm)	Number of Bands	Swath	Revisit Time	Cost
Satellite Sensors						
Landsat 8	15 panchromatic,30 multispectral,100 thermal	430–12510	11	185 km	16 days	Free
Landsat 7	15 panchromatic,30 multispectral,60 thermal	450–12500	8	185 km	16 days	Free
Landsat-5 (TM)	30 multispectral,120 thermal	450–12500	7	185 km	16 days	Free
SPOT-5	2.5 panchromatic,10 multispectral,20 SWIR	480–1750	5	60 km	2–3 days	$
SPOT-6/7	1.5 panchromatic,6 multispectral	455–890	5	60 km	1–3 days	$
Sentinel 2	10, 20 60	490–1375	13	290 km	5 days	Free
WorldView-2	0.46 panchromatic,1.84 multispectral	400–1040	9	16.4 km	1–3 days	$
MODIS	250, 500, 1000	405–14385	36	2330 km	1–2 days	Free
MERIS	300	390–1040	15	1150 km	3 days	Free
QuickBird	0.65 panchromatic, 2.62 multispectral	445–900	5	16.8 km, 18 km	1–3.5 days	$
HICO*	90	350–1080	128	45 km	Irregular	$
HJ-1 A/B	30	430–900	4	360	2 days	$
Airborne Sensors						
AVIRIS	Altitude dependent	400–2500	224	Altitude dependent	N/A	$
ADAR	Altitude dependent	400–1000	4	Altitude dependent	N/A	$
CASI	Altitude dependent	380–1050	288	Altitude dependent	N/A	$
DMSC	Altitude dependent	Varied	Varied	Altitude dependent	N/A	$
PRISM	Altitude dependent	350–1050	>200	Altitude dependent	N/A	$

observed by many vessels during the 2008 Olympic sailing preparations. For the same bloom, another study (Cui et al., 2012) compared satellite-estimated drifting velocity to modelled surface currents as a validation technique in the absence of formal field observations. In all instances, when field data are omitted or substituted, results should be interpreted with caution due to increased uncertainty.

3.3. Image processing

Image processing generally consists of preprocessing, processing, classification, validation, and a generated product. Several software programs are available for imagery processing, including ENVI, PCI Geomatica, ERDAS imagine, eCognition, for spatial data ArcGIS, open source free software packages are also available: QGIS, GRASS, ILWIS, SNAP, and Google's Earth Engine.

3.3.1. Preprocessing

Image preprocessing is the correction of systematic errors and calibration of remotely sensed imagery to produce consistent and comparable data (Schowengerdt, 2012). For macro algae detection, preprocessing steps may differ slightly among studies, but generally include geometric, radiometric, atmospheric correction (for satellite images), and masking of land. These steps are fundamental principals in remote sensing techniques, and thorough descriptions can be found in texts such as Jensen's Introductory Remote Sensing (Jensen, 2005).

3.3.2. Processing

After images have been corrected and masked, information can be extracted with various processing methods. For macro algae detection, common techniques are development of indices, band ratios, and principal component analysis.

3.3.3. Indices and band ratios

Band ratios and spectral indices (Table 3) aid in macro algae detection by enhancing the differences in spectral responses (Dierssen et al., 2015). The normalized difference vegetation index (NDVI), developed for terrestrial vegetation, is also used for macro algae detection due to the spectral similarities between algae and vegetation. NDVI emphasizes the “red-edge” in vegetation and macro algae, and reduces environmental influences (Rouse et al., 1974). This index has been used for detection of *Enteromorpha* blooms in the Yellow Sea (Cui et al., 2012), floating *Sargassum* (Dierssen et al., 2015), and *Macrocystis* biomass (Cavanaugh et al., 2010). Despite the success of NDVI in the aforementioned studies, this index is limited due to its sensitivity to atmospheric effects that can vary throughout the field-of-view (Garcia et al., 2013; Shi and Wang, 2009). Several studies have proposed modified indices to improve upon this limitation (Garcia et al., 2013; Hu, 2009; Huete et al., 1999; Shi and Wang, 2009). Building on indices developed to reduce atmospheric effects and improve the signal from high biomass terrestrial vegetation, Hu (2009) developed the Floating Algae Index (FAI) (Table 3) to detect floating algae with MODIS and Landsat imagery, and found it less sensitive to changes in conditions such as aerosol type, sun glint, and solar geometry compared to other indices.

Similarly, the Normalized Difference Algae Index (NDAI) was developed to detect *Enteromorpha* (Shi and Wang, 2009). NDAI takes into account the NIR and Red reflectance, while also accounting for atmospheric effects by including the influence

Table 3
Indices used for enhancing detection of floating Macro Algae where R = reflectance, SWIR, NIR, Red, Green, Blue indicate the bands from the sensors being used. For full variable definitions, refer to the literature cited.

Index	Equation	Species	Use	Limitations	Study
NDVI: Normalized Difference Vegetation Index	$NDVI = \frac{R_{NIR} - R_{RED}}{R_{NIR} + R_{RED}}$	*Enteromorpha prolifera, Sargassum, Macrocystis*	Emphasize red edge	Sensitive to atmospheric variation in scene	(Cavanaugh et al., 2010; Cui et al., 2012; Dierssen et al., 2015)
FAI: Floating Algae Index	$FAI = R_{rc,NIR} - R'_{rc,NIR}$ $R'_{rc,NIR} = R_{rc,RED} + (R_{rc,SWIR} - R_{rc,RED}) \times (NIR - RED)/(SWIR - RED)$	*Sargassum*	Detect floating algae with MODIS and Landsat	Limited to sensors with certain bands	bib_Hu_2009(Hu, 2009)
NDAI: Normalized Difference Algae Index	$NDAI = \frac{[R_{NIR} - Rayleigh_{NIR}] - [R_{RED} - Rayleigh_{RED}]}{[R_{NIR} - Rayleigh_{NIR}] + [R_{RED} - Rayleigh_{RED}]}$	*Entermorpha prolifera*	Similar to NDVI also takes influence Rayleigh scattering into account	Need SWIR bands at 1240 nm and 2130 nm	Shi and Wang (2009)
SAI: Scaled Algae Index	$SAI = NDVI_{POI} - medianNDVI_{kernel}$	*Ulva prolifera*	Removes background signal from turbidity, sun-glint, and atmospheric effects	Sensitive to the size of the processing kernel	Keesing et al. (2011)
GNDVI: Green Difference Vegetation Index	$GNDVI = \frac{R_{NIR} - R_{GREEN}}{R_{NIR} + R_{GREEN}}$	Cyanobacteria Bloom	Uses green band instead of red for NDVI. Sensitive to chlorophyll variation	Best suited for "green" vegetation	Goldberg et al. (2016)
EVI- Enhanced vegetation index	$EVI = Gain\ Factor \times \frac{(NIR - RED)}{(NIR + C1 \times Red - C2\ x\ Blue + L)}$	*Ulva*	Sensitive to canopy variations	More sensitive to green algae	Son et al. (2012)
MCI- Maximum Chlorophyll Index	$MCI = R_{rc709} - R_{rc681} - (R_{rc754} - R_{rc681})(709 - 681)/(754 - 681)$	*Sargassum*	Measures red-edge reflectance of water column chlorophyll and floating vegetation	Designed for MERIS	(Gower et al., 2006; Hu et al., 2015)
Simple Ratio:NIR/ Blue	$SR = \frac{R_{NIR}}{R_{BLUE}}$	*Nereocystis luetkeana, Alaria*	Detect floating laminaria biomass	Unable to distinguish between species	Stekoll et al. (2006)
Simple ratio: **Red/ Green**	$SR = \frac{R_{RED}}{R_{GREEN}}$	*Submerged laminaria species*	Enhances submerged vegetation	Less effective for canopy detection	Casal et al. (2011)

of Rayleigh scattering. Although FAI and NDAI succeeded in detecting floating macro algae, their use is limited to situations where the effect of Rayleigh scattering can be identified and corrected. To improve upon this limitation, the Scaled Algae Index (SAI) was developed to detect *Ulva* (Keesing et al., 2011). SAI uses a kernel filter to remove a localized background signal that includes turbidity, sun-glint, and atmospheric variation from each pixel, resulting in non-algae pixels having near-zero values, and algae pixels having high contrast with their surroundings.

The FAI, NDAI, and SAI were developed to mitigate the effects of atmospheric and environmental variation throughout large study areas. As such, these indices are especially suited for large-scale studies that target macro algae covering areas in the hundreds of metres, capable of being detected with medium to coarse spatial resolution imagery such as MODIS. Due to the growth patterns of bull kelp, which limit its distribution to relatively small areas close to the coastline, atmospheric differences throughout the study area are not as significant as those in the large, open-ocean areas typical of MODIS imagery. However, coastal areas may experience large spatial variations in turbidity, which may be reduced using the SAI index derived from high-resolution imagery, and modifications of FAI and NDAI using alternative bands on high-resolution sensors may be useful for detecting bull kelp.

Depending on the characteristics of the survey area, indices created for other applications have been useful for detecting floating macro algae. Casal et al. (2011) experimented with multiple band ratio combinations to detect submerged kelp using a band ratio of Red over Green. Augenstein et al. (1991) used a simple ratio of NIR over Red, and Deysher (1993) used NIR over Green band to detect *Macrocystis*. Depending on the site conditions and band availability of the sensor used, substitutions of

bands from established indices may produce better results such as in Stekoll et al. (2006) using the Blue band instead of the Red band in the NDVI to detect *Nereocystis* and *Alaria*.

3.3.4. Principal component analysis

Principal component analysis (PCA) is a statistical technique used to reduce variance and dimensionality of a data set by transforming image bands into a set of uncorrelated output products, each composed of a combination of the original bands. The first principal component (PC1) represents the maximum proportion of variance from the data, and each subsequent PC represents the maximum of the remaining variance. This allows patterns in the data to be identified by accentuating similarities and differences (Gupta et al., 2013). For the purpose of macro algae detection, PCA is beneficial for reducing spectral noise, and increasing separability between macro algae and its surroundings, which ultimately aids in image classification. Cavanaugh et al. (2010) found useful information in the different principal components of SPOT 5 imagery: the PC1 accounted for variations in atmosphere, suspended particles, whitecaps, and waves, and PC2 showed a signal that was inversely consistent with the expected kelp reflectance and could be used to delineate the canopy.

3.3.5. Classification

Classification of image data results in a spatial representation of kelp aerial extent, which can then be used to derive products such as biomass, productivity or temporal change, or persistence trends. There are several methods of classification that have been applied in previous research: supervised and unsupervised classification algorithms, thresholds, object-oriented segmentation, spectral un-mixing, and manual visual classification. Finally, the results of a classification may need to be adjusted to remove errors caused by speckling or noise. The final classification results are validated using ground-truth-based accuracy assessments.

3.3.6. Supervised classification

Supervised classification uses ground-truth data provided by the user to train a classifier according to the classes of interest. This method is best used when the user has high quality field data and wishes to classify several cover types. Various supervised classification techniques have been used in macro algae studies, including Spectral Angle Mapper (SAM) and maximum likelihood. The SAM method groups pixels into classes based on the angle in spectral space between the value of a given pixel and the class spectra (Anderson et al., 2007). The maximum likelihood classification calculates the probability that a given pixel belongs to a class previously characterized with training data, with the assumption that each class is normally distributed (Casal et al., 2011; Hogland et al., 2017). Minimum distance classification is similar to maximum likelihood except that it allows for the use of classes that are not normally distributed (Richards, 2013).

3.3.7. Image threshold

Using image thresholds is a simple technique where threshold values are defined based on the separability of the features of interest. For example, a threshold value from an original band, PC product, or index is applied to the image, resulting in a binary product wherein each pixel is identified as either above or below that value. The threshold value may be determined through defining the value that produces the best output, as compared to validation data or visual interpretation of the satellite image (Cui et al., 2012; Kim et al., 2010), based on sensitivity analysis (Garcia et al., 2013) or spatial gradient analysis (Hu, 2009). A basic threshold will produce a binary product of either “kelp” or “not kelp.”

Threshold-based approaches may also consider a stepwise or decision tree procedure that can identify floating macro algae by ruling out other spectral features (Hu et al., 2015). For example, to discriminate *Sargassum* from floating seagrass wrack, Dierssen et al. (2015) applied a stepwise rule with multiple index/band thresholds to first isolate pixels containing floating vegetation (“vegetation” or “not vegetation”), and then applied a second index threshold to the vegetation class to differentiate between *Sargassum* and seagrass. In any threshold approach, a major challenge is threshold variability throughout the image, which can sometimes be dealt with by scaling image pixels using a kernal-based approach and then applying a global threshold (Garcia et al., 2013).

3.3.8. Spectral un-mixing

Due to limitations in spatial resolution of images acquired by satellite and the small size of some floating macro algae beds, pixel reflectance may represent a mixture of signals composed of the target algae and the surrounding seawater. For example, in a binary classification of floating macro algae, a mixed pixel would be classified as either algae or water, and therefore inaccuracy in canopy extent and biomass estimations may occur. Cavanaugh et al. (2011) and Bell et al. (2015b) used Multiple Endmember Spectral Mixture Analysis (MESMA) to address this problem by modelling each pixel in a Landsat image as a linear combination of giant kelp and seawater using one kelp pixel and multiple representative water pixels. MESMA was then used to determine the percent of kelp in each pixel. Uhl et al. (2013) used hyperspectral data to determine whether various species of macro algae could be detected within a mixed pixel and found that, while species level un-mixing was not possible due to the similarities in reflectance, higher taxonomic levels could be distinguished. For bull kelp detection, spectral un-mixing approaches may be especially advantageous given the small size of the kelp beds compared to the spatial resolution of available satellite imagery.

3.3.9. Object Based Image Analysis

Object Based Image Analysis (OBIA) is a method of classification in which pixels are first grouped into image objects (Blaschke, 2010). This technique is especially useful in conditions where the spatial resolution of an image is very high compared to the scale of the target of interest, such as in aerial, UAV, or high resolution satellite images (Blaschke, 2010; Nahirnick et al., 2018). Instead of classifying images on a pixel-by-pixel basis, image objects are created from groups of adjacent pixels based on information from spectral bands and contextual information, such as shape, scale, and compactness. This method can also include other spatial information, such as benthic substrate or bathymetry. Each object can be composed of pixels with similar digital values and is thus spectrally more homogeneous within the object than between neighbours (Yu et al., 2006). After segmentation, objects are classified according to a combination of various object features, such as mean, median, standard deviation, dissimilarity, homogeneity, texture, or spatial relationship to other objects (Blaschke, 2010; Yu et al., 2006).

3.3.10. Visual interpretation

Visual interpretation techniques can be applied to any type of imagery (Donnellan and Foster, 1999), including images produced from transformed bands or indices (Casal et al., 2011). This method relies on a user to visually define and delineate the boundaries of kelp beds. While visual interpretation benefits from its simplicity, it is subjective and may therefore introduce error. Furthermore, as a non-automated process, it may be more time-consuming and less repeatable than other classification techniques (Pfister et al., 2017).

3.3.11. Unsupervised classification

Unsupervised classification algorithms do not require ground-truth information for training. A commonly used algorithm, cluster analysis, groups pixels into classes based on their spectral similarities, and then assigns all possible pixels to the nearest class (Tou and Gonzalez, 1974). A key consideration is the number of classes selected as an output, which will depend on the amount of variability in a survey area, where masked images with mostly kelp and water will need fewer classes than an area with other features such as rocks, boats, docks, etc. A small number of classes may group kelp with other spectrally similar features in the image, while a large number of classes may divide kelp into several clusters due to differences in density. Clustering algorithms have been effectively used for kelp classification of both aerial (Deysher, 1993) and satellite imagery (Casal et al., 2011).

3.3.12. Classification adjustment

Often, the outputs from classifications contain errors caused by digital noise in the image, or classified artifacts that may need to be removed. For example, Cavanaugh et al. (2010) applied a filter wherein single isolated kelp pixels were assumed to be incorrect and reclassified as water. The applicability of this technique depends on the spatial resolution of the sensor and the size of the kelp beds, where errors in classifying small kelp beds will be more difficult to determine.

3.3.13. Validation and accuracy assessment

To evaluate the extent of errors associated with the classification step, an estimate of the overall accuracy is usually necessary, allowing the classification products to be used in decision-making processes (Richards and Congalton, 2001). In order to assess accuracy, ground-truth data must exist, which ideally should be collected at the same time as image acquisition. When data are not collected at the same time as image acquisition, close attention must be paid to differences in tide height, current, and season, as these factors can have major impacts on the mapped extent of macro algae (Britton-Simmons et al., 2008).

The accuracy of a classification is generally reported in terms of Producers accuracy (errors of commission) and Users accuracy (errors of omission). These errors are defined based on comparison between classification outputs and validation data (i.e., ground-truth) and creating a standard error matrix to report omission and commission errors (Congalton, 1991). The total accuracy is also commonly reported, and is found by dividing the total number of correctly classified pixels by the total number of pixels considered. A poor outcome from an error matrix may induce reiteration through the classification steps until a satisfactory outcome is achieved, if possible.

3.3.14. Products

The goals of a monitoring project may include kelp detection (presence/absence), quantification of the spatial extent of beds, change detection, or deriving biological parameters such as biomass, productivity, and physiological condition. Basic kelp detection products can be used for temporal analysis or for biomass estimates. For detecting temporal trends, multiple classification products derived from images collected at different times are used; however, care must be taken concerning differences in image quality and conditions at the time of imagery acquisition that may affect the accuracy of kelp classification between time periods. Differences in tide, water surface, and water column characteristics may create error in the classified extent of kelp that is not due to the full kelp extent (Britton-Simmons et al., 2008). To overcome some of these differences, images should be normalized when possible.

Monitoring initiatives that require biomass estimates can give more detailed insight into kelp forest productivity and response to environmental change (Bell et al., 2015a). To calculate biomass from imagery, physical data such as plant densities, lengths, and weights need to be collected at an appropriate scale (Cavanaugh et al., 2010). This information is then

related to image derived indices such as NDVI values (Cavanaugh et al., 2010) or kelp fraction (Bell et al., 2015b) through linear regression. Total or surface kelp biomass can then be calculated from the classified kelp area (Bell et al., 2015a; Cavanaugh et al., 2010; Stekoll et al., 2006). In California, biomass of giant kelp beds was derived from Landsat imagery using the MESMA method discussed above, where the percent cover of kelp in each 30 m pixel was related to diver estimates of kelp density using a linear regression (Cavanaugh et al., 2011). Other measures such as sub-bulb diameter of bull kelp have been used to estimate plant weight, enabling a simpler method of field data collection for use in derived biomass estimates (Stekoll et al., 2006).

4. Case study: remote sensing of bull kelp in the Salish Sea

This section presents a case study in which methods adapted from the macro algae studies discussed in sections 2 and 3 are adopted for mapping fringing beds of bull kelp in nearshore regions of the Salish Sea on the west coast of Canada.

4.1. Study site

The study site covers approximately 100 km^2 in Cowichan Bay and Sansum Narrows in the Salish Sea, on the west coast of Canada (Fig. 4). In this region, bull kelp is the dominant canopy forming algae often growing in narrow fringing beds along steep rocky shorelines, at depths between 0 and 20 m (Mumford, 2007). Most growth occurs between April and early September, depending on water and light conditions (Mumford, 2007; Springer et al., 2007). Canopies may be maintained until fall or early winter depending on the sea and temperature conditions (Springer et al., 2007).

4.2. Methods

4.2.1. Step 1: imagery acquisition and ground-truthing

A WorldView 3 satellite image covering approximately 100 km^2 with four multispectral bands (480, 545, 660, 832 nm) and 1.8 m spatial resolution was planned for acquisition by DigitalGlobe on August 30th, 2016. Conditions required for successful collection were: tide height lower than 1.2 m MLLW, specified by the ground-truth methods as the tide height where the majority of the kelp canopy should be visible at the surface; sensor angle less than 15 degrees off nadir; minimal cloud cover (<5% over shoreline); and low wind conditions (<10 m/s).

At the same time that image collection occurred, ground-truthing of kelp extent over a subset of the area was conducted using kayak and handheld GPS methods following Fretwell and Boyer (2010). Three teams of two person crews started from different locations and paddled kayaks along the shoreline for 1 h before, during, and 1 h after the low slack tide of 1.1 m MLLW. Kelp location was recorded by handheld GPS (Garmin 64s) as either a point (single bulb, or several bulbs in close proximity <1 m^2), line (continuous kelp less than 5 m wide), or polygon (continuous kelp more than 5 m wide). Beds were considered distinct if there was a distance greater than 8 m between kelp plants. All data was digitized in ArcGIS into shapefiles for use as training and validation data.

4.2.2. Step 2: pre-processing

Initially, the acquired image was georectified in BC Albers NAD 83 with ArcGIS 10.5 using 30 ground control points, producing a final average root mean square error (RMSE) of 0.28 m. Next, the raw digital numbers were converted to at-

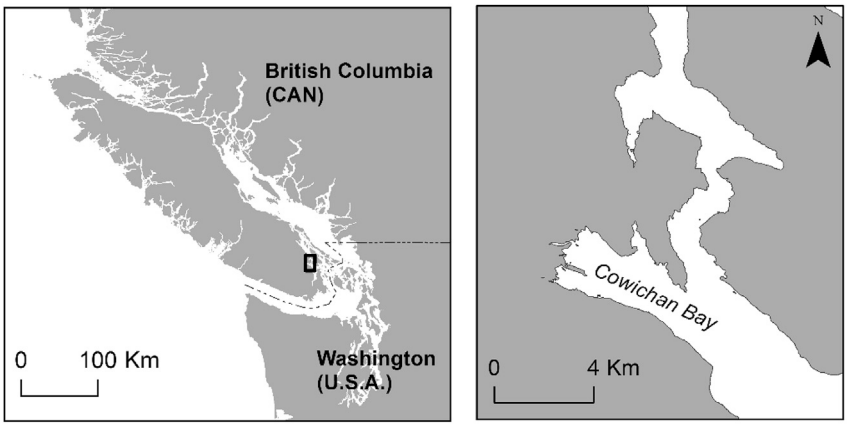

Fig. 4. Left: Regional context of study area (black box) Cowichan Bay and Sansum Narrows on the east coast of Vancouver Island, British Columbia, Canada. Right: extent of study area, covering Cowichan Bay and Sansum Narrows.

satellite radiance (L_λ in units of $\mu W/cm^{-2}\ sr^{-1}\ nm^{-1}$ equation (1)), and an absolute atmospheric correction was applied using the FLAASH® (Fast Line of Sight using Hypercubes) tool in ENVI (Matthew et al., 2000).

$$L_\lambda = Gain^{*}Pixel\ value + Offset \quad (1)$$

A land mask was created using object-based segmentation with Definiens eCognition to allow for separation of land from water; the NIR, Red, and Green bands were used as inputs, and spectral characteristics were given greater weight than spatial characteristics for defining objects. This method resulted in a more accurate definition of the coastline than the use of published coastline shapefiles, which do not reflect the tide level occurring at the time of image acquisition. A 4-m buffer was added to the defined land mask to account for occurrence of nearshore vegetation such as *Fucus* and *Ulva*, as well as removal of adjacency effects and pixel mixing caused by the proximity of terrestrial vegetation to the shoreline. While this method produces a reliable mask of the exact shoreline location, and thus allows for effective masking of land classes that may influence the classification, it will also potentially mask kelp located within 4 m of the shoreline. Kelp in such close proximity to the shoreline is not likely to be resolved from other algae species in the nearshore due to similarities in reflectance. It is preferable to mask this area rather than to misclassify the shoreline algae as kelp. Finally, a 30 m deep-water mask was applied using bathymetry contours created from single and multi-beam sonar data acquired from the Canadian Hydrography Service for coastal British Columbia. This mask represents the depth at which kelp will not be found in this region (Springer et al., 2007). Together, the masks minimize erroneous classification introduced from land, shoreline algae, glint, waves, and water column constituents.

4.2.3. Step 3: image processing

4.2.3.1. Index selection. To explore the best possible bands and band ratios for separating kelp from other features, the Jeffries-Matusita Distance (JMD) statistical separability analysis (Swain and King, 1973) was applied to all the applicable indices and transformations available in the literature (Table 3). Some indices discussed in the literature could not be applied due to the limitations of band availability for the WorldView 3 image. The following products were analyzed: NDVI, GNDVI, SAI, EVI, simple ratios as well as PC outputs, and the Blue, Green, Red, and NIR reflectance bands. According to the JMD analysis, the products selected as best able to identify kelp → NDVI, GNDVI, and PC1 → were further linearly enhanced to maximize spectral differences and minimize noise, and then used as input for classification.

4.2.4. Step 4: classification

To illustrate the feasibility of using different classification techniques with different levels of user input, four types of supervised methods, minimum distance (MD), decision tree threshold (DT), spectral un-mixing (SU), and object-based image

Table 4
Error matrices for Minimum Distance (MD), ISODATA (ISO), Decision Tree (DT) spectral unmixing SU, and OBIA classification results for bull kelp in the Salish Sea.

			Ground-truth				Total Accuracy
			Kelp	Not Kelp	Total	User Accuracy	
Classification	MD	Kelp	409	42	451	90.7	90.7
		Not Kelp	37	358	395	90.6	
		Total	446	400	846		
		Producers Accuracy	91.7	89.5			
	ISO	Kelp	376	83	459	81.9	86.9
		Not kelp	28	362	390	92.8	
		Total	404	445	849		
		Producers Accuracy	93.1	81.4			
	DT	Kelp	385	75	460	83.7	87.9
		Not Kelp	27	359	386	93.0	
		Total	412	434	846		
		Producers Accuracy	93.5	82.7			
	SU	Kelp	399	62	461	86.6	88.5
		Not Kelp	34	343	377	91.0	
		Total	433	405	838		
		Producers Accuracy	92.2	84.7			
	OBIA	Kelp	333	121	454	73.4	82.5
		Not Kelp	27	364	391	93.1	
		Total	360	485	845		
		Producers Accuracy	92.5	75.1			

analysis (OBIA), and one unsupervised method, ISODATA (ISO), were compared. All classifications used a composite of NDVI, GNDVI, and PC1 as input.

For the supervised methods, MD used training data derived from ground-truth and expert knowledge to define six classes (kelp, water, glint, shallow water, bright objects, and shadow) with at least 100 pixels each. The DT used thresholds defined by the mean of the same class samples ±2 standard deviations. The SU was defined based on adapted methods from Cavanaugh et al. (2011), in which the *matched filtering* tool in ENVI was used to un-mix pixels. Spectral endmembers for dense kelp (50 kelp endmembers) and water (120 water endmembers) were selected from the image based on ground-truth data and known reflectance characteristics of kelp and water. The result is a grey scale image for each endmember representing their approximate subpixel abundances, where a value of 1.0 would represent 100% kelp. Based on the ground-truthing data and known spectral reflectance of kelp and water, a kelp minimum fraction threshold of 0.142 was defined. All pixels with a fraction lower than 0.142 were classified as water. OBIA was applied using Definiens eCognition® Version 8. As commonly used in object-based classification, trials for different weights for parameters of scale, shape, and compactness were conducted to determine the optimal approach for the segmentation (Evans et al., 2014). Defined parameters were considered acceptable if areas of known kelp beds were captured as a single object, rather than broken into several objects or combined with areas of non-kelp. The resulting image objects were classified using a supervised nearest-neighbour approach for the six classes defined above. For the unsupervised ISO method, multiple classification trials were performed to define the combination of parameters and number of classes needed to yield the best results.

4.2.5. Step 5: accuracy assessment

The output product of each classification was converted into two binary classes, kelp and non-kelp, where all non-kelp classes defined through classification were combined into one class. A stratified random sample approach was used to define 500 validation pixels per class from the ground-truth data, and an error matrix was produced (Table 4). The selection of the validation pixels also considered the uncertainties in the ground-truth data due to the accuracy of the handheld GPS (±9 m), displacement of kelp beds of up to 1 m related to changes in tide and current and bias or inaccuracy of the kayak surveyors. A 10 m buffer was added to the kelp ground-truth polygons (Fig. 6) to accommodate for these possible uncertainties, and no samples in this region were used for either the kelp or the non-kelp classes, reducing the number of pixels for validation to a range between 400 and 485 for each class.

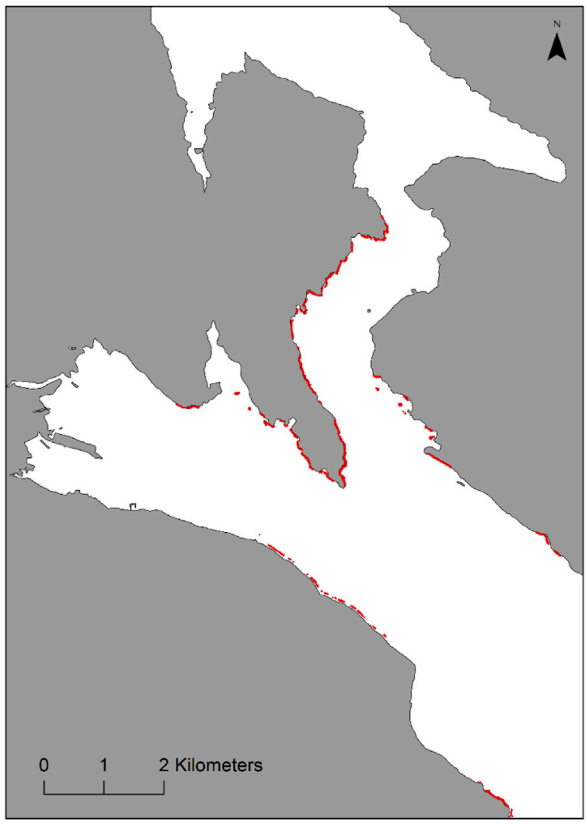

Fig. 5. Result of minimum distance (MD) supervised classification with total accuracy of 90.7.

4.3. Results and discussion

All five classification methods performed relatively well in detecting kelp beds. For total accuracy, MD (90.7%) and SU (88.5%) yielded the best results (Fig. 5), followed by DT (87.9%), ISO (86.9%), and OBIA (82.5%) (Table 4). The classification products showed high fidelity when visually compared to the shape and location of ground-truth maps (Figs. 6 and 7), and the total accuracies are comparable to other studies which reported values between 74% and 94%, depending on the density of the kelp (Casal et al., 2011; Fyfe et al., 1999).

For all classification outputs, accuracy was generally the highest in areas where kelp was dense and beds were large, as illustrated in Figs. 6 and 7. In these regions, the detected spectral signals better represent kelp due to less mixing with the spectral signal of water (see Fig. 1 for spectral signal of dense kelp vs sparse kelp). Conversely, in areas where kelp was sparse, kelp detection was less reliable due to spectral signal mixing with water. The greatest error happened in areas in which

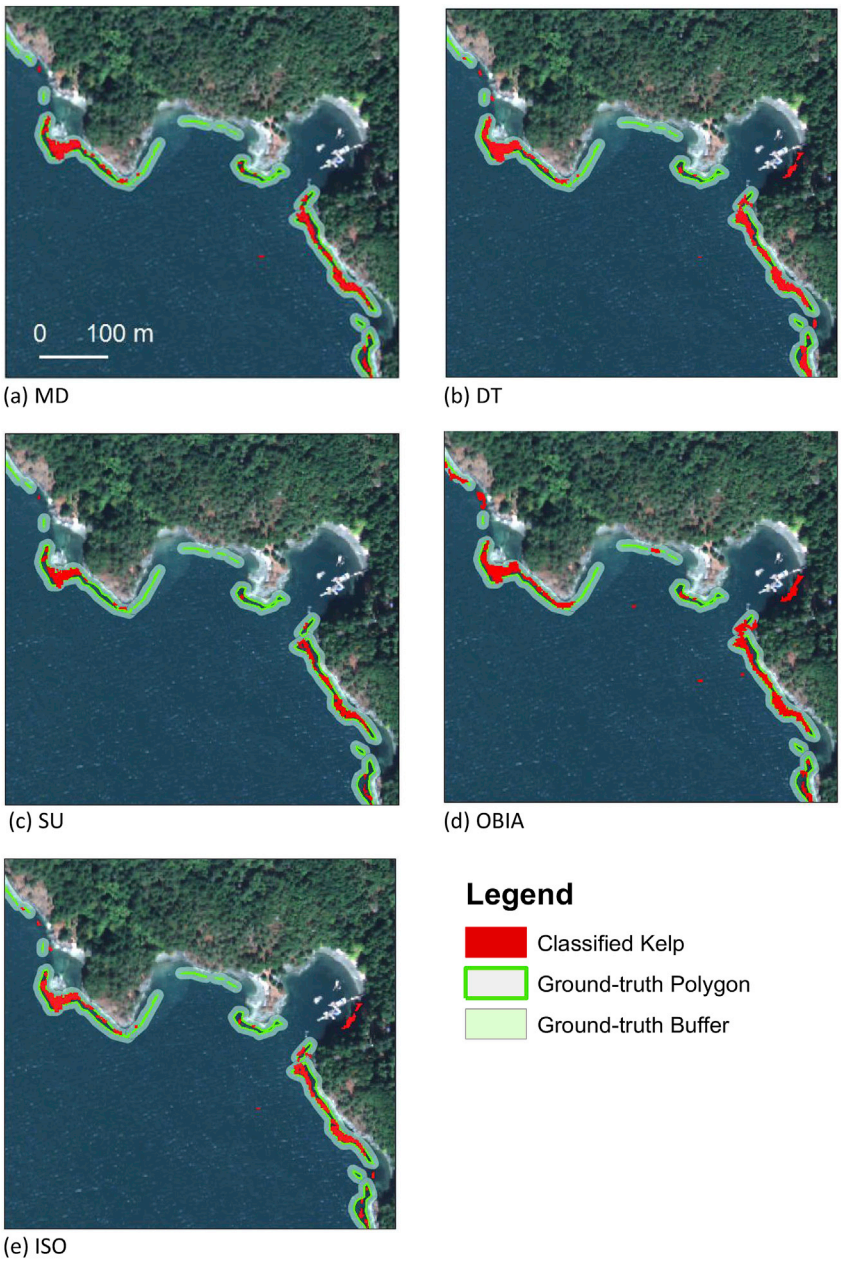

Fig. 6. Classification results for the MD, DT, SU, OBIA, and ISO classifications on a subset of the true colour WorldView 3 image for bull kelp in the Salish Sea. (For interpretation of the references to colour in this figure legend, the reader is referred to the Web version of this article.)

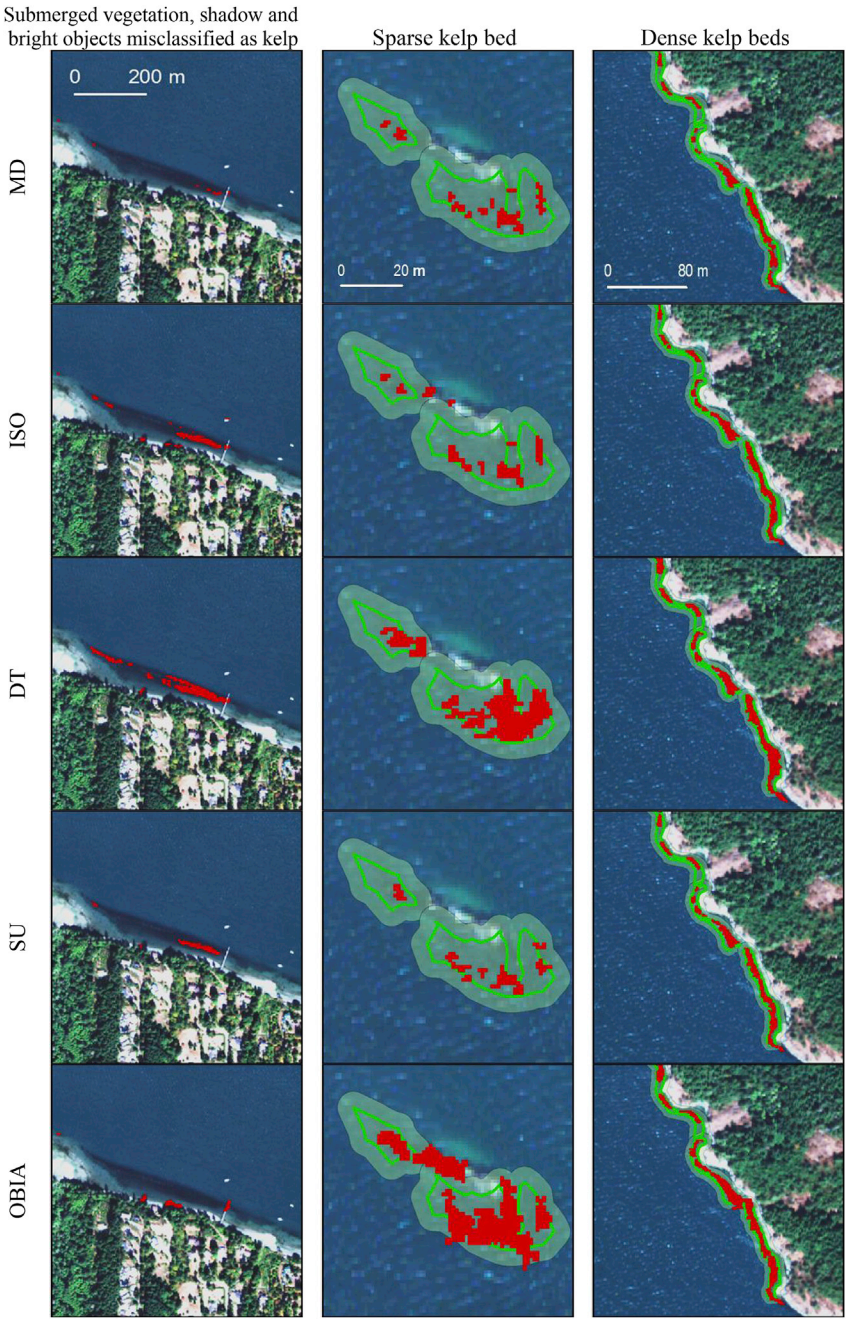

Fig. 7. Errors in classification methods for submerged vegetation, shadow, bright objects, sparse kelp beds, and dense kelp beds in the Salish Sea (Legend provided in Fig. 6).

submerged vegetation such as eelgrass was classified as kelp. The reflectance spectra of submerged kelp and eelgrass with high epiphytes loads are very similar when using only four spectral bands (O'Neill and Costa, 2013). Alternatives for minimizing this error include using hyperspectral data to improve the spectral separability between species and/or masking areas of soft substrate where kelp is unlikely to occur. Misclassification also occurred between the shadow of terrestrial vegetation on the water, as seen in Fig. 6. Despite the 4 m buffer, the shadow of terrestrial vegetation was not removed in some areas during the masking process, likely due to large shadows caused by the height of trees, sensors viewing angle, and sun illumination angle (Fig. 7).

Among the supervised methods, the MD classification produced the best results due to its use of high-quality ground-truth data and consideration of the mean of training classes in the minimum distance algorithm. Similarly, the spectral un-mixing

Table 5
Selection of classification methods based on quality of input parameters.

Data Quality	Study Site Characteristics	Ground-truth Data	Sensor Type and Resolution	Classification Type
Ideal	Large dense kelp beds, far from shoreline	Collected at same day and time as imagery	Mid-high resolution 30 m −2m	OBIA, MD, SU, DT, ISO
	Large sparse beds, small beds, near shoreline	Collected during same season	High resolution (<10 m)	MD, SU, DT, ISO
Poor	Small beds, fringing, close proximity to shoreline	No ground-truth	High resolution 2 m	ISO

method yielded good results. In this method, the best results will occur when pure pixels of each class are used to establish the un-mixing algorithm. The decision tree classification applied user-defined thresholds to classify pixels, which can introduce bias on class definition. Adjusting threshold values or including additional classes where misclassifications occur may improve the results. The poorest results were obtained with the OBIA approach. The small size, irregular shape, and sparse nature of the kelp beds resulted in objects containing a range of kelp and water extents. In these conditions, the mean of each object mostly represents the mixing of spectral signals corresponding to water and kelp. Depending on ratio of kelp and water, image objects containing kelp may be classified as water, thus causing larger error compared to pixel-based classification. In areas where kelp beds are large and dense, OBIA will likely perform better as image objects will more accurately represent kelp spectral signatures and have a uniform nature. The unsupervised ISODATA method performed well with both dense and sparse kelp beds, as the iterative clustering algorithm is most affected by the difference in spectral signals between cover types rather than their spatial relationship. This method is advantageous where there is a lack of ground-truth data, such as when analyzing historical imagery. However, knowledge of the site characteristics or spectral signature of cover types is still required to label the resulting classes.

Table 5 summarizes the choice of image classification methods based on the characteristics of the study sites and available ground-truth information. Specifically, sensors will depend on the size and location of beds, where large offshore beds can be detected with medium resolution sensors and smaller nearshore beds will require higher resolution imagery. As kelp beds become sparse, fringing, or small, classification techniques such as supervised minimum distance yield the most robust results. Additionally, the quality of the ground-truth data affects the choice of classification method, with high quality data acquired concurrent to image acquisition being ideal for all classification techniques. If ground-truth data is unavailable, unsupervised ISODATA classification is the most appropriate choice. However, for any of the classification approaches, environmental conditions during the time of image acquisition, including tide height, currents, water surface roughness, turbidity, and sensor angle will also have effects on the accuracy of the classifications.

5. Conclusions

Remote sensing technologies and imagery processing methods are continuously advancing, allowing for improvements in macro algae detection. Specifically, for kelp mapping and biomass indicators, ongoing research is developing new techniques for deriving ecological information from remotely sensed kelp beds. With increasing sources of high-quality data, automated classification methods are being developed for use with free data sources such as Landsat (Bell et al., 2018; Nijland et al., 2019), allowing for long term monitoring and detection of large kelp beds with global scale potential. Ultimately, these data sets are crucial to understanding environmental drivers of kelp distribution and abundance, and how they relate to ecosystem functions affecting biodiversity, community structure, and productivity.

With the growing availability of high spatial resolution images, such as WorldView, SPOT, and GeoEye sensors, the accuracy of detecting small patches of fringing kelp along nearshore zones has increased. However, for successful use of remote sensing, considerations concerning the environmental conditions at the time of image collection, such as tide height, currents, waves, kelp extent, and imagery analysis techniques are of utmost importance. Additionally, the scale of areas able to be studied may be limited by the smaller coverage and greater costs of higher resolution imagery. Here, we present a literature review and a case study demonstrating how high-resolution satellite imagery can be used effectively for mapping at regional scales by applying imagery-processing techniques adapted from the literature. By using appropriate methods suited to the characteristics of the area of interest, we are able to accurately detect floating kelp beds and create maps of kelp distribution for nearshore systems. Specifically, among the evaluated indices and classification methods, the supervised minimum distance classifier with input of NDVI, GNDVI, and PC1 produced the map with the highest accuracy (90.7%). For monitoring that requires temporal analysis without ground-truth data, unsupervised ISODATA can also produce accurate results. This case study illustrates a systematic method that can be transferred to others areas of the world where species form small or fringing beds.

Funding

This study was supported Pacific Salmon Foundation (PSF) as part of the Salish Sea Marine Survival Project (SSMSP) and NSERC USRA [Dupont].

Acknowledgements

This is publication number 30 from the Salish Sea Marine Survival Project (marinesurvivalproject.com). Funding was provided by the Pacific Salmon Foundation and NSERC USRA. We would like to thank SeaChange Marine Conservation Society, Cowichan Tribes, Mayne Island Conservancy Society and the Pender Island Conservancy Association for their invaluable contributions collecting ground-truth data.

References

Amsler, C.D., Neushul, M., 1989. Diel periodicity of spore release from the kelp Nereocystis luetkeana (Mertens) Postels et Ruprecht. J. Exp. Mar. Biol. Ecol. 134, 117–127. https://doi.org/10.1016/0022-0981(90)90104-K.

Anderson, J.M., Barrett, J., Wolstenhome, G.E.W., Fitzsimons, D.W., 1979. Chlorophyll-protein complexes of Brown algae: P700 reaction centre and light-harvesting complexes. In: Chlorophyll Organization and Energy Transfer in Photosynthesis, pp. 81–104. https://doi.org/10.1002/9780470720431.ch4.

Anderson, R.J., Rand, A., Rothman, M.D., Share, A., Bolton, J.J., 2007. Mapping and quantifying the South African kelp resource. Afr. J. Mar. Sci. 29, 369–378. https://doi.org/10.2989/AJMS.2007.29.3.5.335.

Augenstein, E.W., Stow, D.A., Hope, A.S., 1991. Evaluation of spot hrv-xs data for kelp resource inventories. Photogramm. Eng. Rem. Sens. 57, 501–509.

Babin, M., Stramski, D., Ferrari, G.M., Claustre, H., Bricaud, A., Obolensky, G., Hoepffner, N., 2003. Variations in the light absorption coefficients of phytoplankton, nonalgal particles, and dissolved organic matter in coastal waters around Europe. J. Geophys. Res. 108, 3211. https://doi.org/10.1029/2001jc000882.

Bell, T.W., Allen, J.G., Cavanaugh, K.C., Siegel, D.A., 2018. Three decades of variability in California's giant kelp forests from the Landsat satellites. Remote Sens. Environ. (in press) https://doi.org/10.1016/j.rse.2018.06.039.

Bell, T.W., Cavanaugh, K.C., Reed, D.C., Siegel, D.A., 2015a. Geographical variability in the controls of giant kelp biomass dynamics. J. Biogeogr. 42, 2010–2021. https://doi.org/10.1111/jbi.12550.

Bell, T.W., Cavanaugh, K.C., Siegel, D.A., 2015b. Remote monitoring of giant kelp biomass and physiological condition: an evaluation of the potential for the Hyperspectral Infrared Imager (HyspIRI) mission. Remote Sens. Environ. 167, 218–228. https://doi.org/10.1016/j.rse.2015.05.003.

Blaschke, T., 2010. Object based image analysis for remote sensing. ISPRS J. Photogrammetry Remote Sens. 65, 2–16. https://doi.org/10.1016/j.isprsjprs.2009.06.004.

Brezonik, P.L., Olmanson, L.G., Finlay, J.C., Bauer, M.E., 2015. Factors affecting the measurement of CDOM by remote sensing of optically complex inland waters. Remote Sens. Environ. 157, 199–215. https://doi.org/10.1016/j.rse.2014.04.033.

Britton-Simmons, K., Eckman, J.E., Duggins, D.O., 2008. Effect of tidal currents and tidal stage on estimates of bed size in the kelp Nereocystis luetkeana. Mar. Ecol. Prog. Ser. 355, 95–105. https://doi.org/10.3354/meps07209.

Byrnes, J.E., Reed, D.C., Cardinale, B.J., Cavanaugh, K.C., Holbrook, S.J., Schmitt, R.J., 2011. Climate-driven increases in storm frequency simplify kelp forest food webs. Glob. Chang. Biol. 17, 2513–2524. https://doi.org/10.1111/j.1365-2486.2011.02409.x.

Casal, G., Kutser, T., Domínguez-Gómez, J.A., Sánchez-Carnero, N., Freire, J., 2013. Assessment of the hyperspectral sensor CASI-2 for macroalgal discrimination on the Ría de Vigo coast (NW Spain) using field spectroscopy and modelled spectral libraries. Cont. Shelf Res. 55, 129–140. https://doi.org/10.1016/j.csr.2013.01.010.

Casal, G., Sánchez-Carnero, N., Sánchez-Rodríguez, E., Freire, J., 2011. Remote sensing with SPOT-4 for mapping kelp forests in turbid waters on the south European Atlantic shelf. Estuar. Coast Shelf Sci. 91, 371–378. https://doi.org/10.1016/j.ecss.2010.10.024.

Cavanaugh, K.C., Siegel, D.A., Kinlan, B.P., Reed, D.C., 2010. Scaling giant kelp field measurements to regional scales using satellite observations. Mar. Ecol. Prog. Ser. 403, 13–27. https://doi.org/10.3354/meps08467.

Cavanaugh, K.C., Siegel, D.A., Reed, D.C., Dennison, P.E., 2011. Environmental controls of giant-kelp biomass in the santa barbara channel, California. Mar. Ecol. Prog. Ser. 429, 1–17. https://doi.org/10.3354/meps09141.

Charrier, B., Le Bail, A., de Reviers, B., 2012. Plant Proteus: brown algal morphological plasticity and underlying developmental mechanisms. Trends Plant Sci. 17, 468–477. https://doi.org/10.1016/J.TPLANTS.2012.03.003.

Christie, H., Norderhaug, K.M., Fredriksen, S., 2009. Macrophytes as habitat for fauna. Mar. Ecol. Prog. Ser. 396, 221–233. https://doi.org/10.3354/meps08351.

Congalton, R.G., 1991. A review of assessing the accuracy of classifications of remotely sensed data. Remote Sens. Environ. 37, 35–46. https://doi.org/10.1016/0034-4257(91)90048-B.

Cui, T.W., Zhang, J., Sun, L.E., Jia, Y.J., Zhao, W., Wang, Z.L., Meng, J.M., 2012. Satellite monitoring of massive green macroalgae bloom (GMB): imaging ability comparison of multi-source data and drifting velocity estimation. Int. J. Remote Sens. 33, 5513–5527. https://doi.org/10.1080/01431161.2012.663112.

Deiman, M., Iken, K., Konar, B., 2012. Susceptibility of Nereocystis luetkeana (Laminariales, ochrophyta) and eualaria fistulosa (Laminariales, ochrophyta) spores to sedimentation. ALGAE 27, 115–123. https://doi.org/10.4490/algae.2012.27.2.115.

Dethier, M.N., Raymond, W.W., McBride, A.N., Toft, J.D., Cordell, J.R., Ogston, A.S., Heerhartz, S.M., Berry, H.D., 2016. Multiscale impacts of armoring on Salish Sea shorelines: evidence for cumulative and threshold effects. Estuar. Coast Shelf Sci. 175, 106–117. https://doi.org/10.1016/j.ecss.2016.03.033.

Deysher, L.E., 1993. Evaluation of remote sensing techniques for monitoring giant kelp populations. Hydrobiologia 260/261, 307–312. https://doi.org/10.1007/BF00049033.

Dierssen, H.M., Chlus, A., Russell, B., 2015. Hyperspectral discrimination of floating mats of seagrass wrack and the macroalgae Sargassum in coastal waters of Greater Florida Bay using airborne remote sensing. Remote Sens. Environ. 167, 247–258. https://doi.org/10.1016/j.rse.2015.01.027.

Donnellan, M.D., Foster, M.S., 1999. Effects of Small-Scale Kelp Harvesting on Giant Kelp Surface Canopy Dynamics in the Ed Ricketts Underwater Park Region, Final Report to the Monterey Bay National Marine Sanctuary and the Cities of Monterey and Pacific Grove.

Druehl, L.D., 1970. The pattern of Laminariales distribution in the northeast Pacific. Phycologia 9, 237–247. https://doi.org/10.2216/i0031-8884-9-3-237.1.

Duffy, J.P., Pratt, L., Anderson, K., Land, P.E., Shutler, J.D., 2018. Spatial assessment of intertidal seagrass meadows using optical imaging systems and a lightweight drone. Estuar. Coast Shelf Sci. 200, 169–180. https://doi.org/10.1016/j.ecss.2017.11.001.

Dugan, J.E., Hubbard, D.M., Page, H.M., Schimel, J.P., 2011. Marine macrophyte wrack inputs and dissolved nutrients in beach sands. Estuar. Coasts 34, 839–850. https://doi.org/10.1007/s12237-011-9375-9.

Duggins, D., Eckman, J.E., Siddon, C.E., Klinger, T., 2001. Interactive roles of mesograzers and current flow in survival of kelps. Mar. Ecol. Prog. Ser. 223, 143–155. https://doi.org/10.3354/meps223143.

Duggins, D.O., 1988. The effects of kelp forests on nearshore environments: biomass, detritus, and altered flow. In: VanBaricom, G.R., Estes, J.A. (Eds.), The Community Ecology of Sea Otters. Ecological Studies (Analysis and Synthesis). Springer, Berlin, Heidelberg, pp. 192–201. https://doi.org/10.1007/978-3-642-72845-7_9.

Eckman, J.E., Duggins, D.O., Sewell, A.T., 1989. Ecology of under story kelp environments. I. Effects of kelps on flow and particle transport near the bottom. J. Exp. Mar. Biol. Ecol. 129, 173–187. https://doi.org/10.1016/0022-0981(89)90055-5.

Evans, T.L., Costa, M., Tomas, W.M., Camilo, A.R., 2014. Large-scale habitat mapping of the Brazilian Pantanal wetland: a synthetic aperture radar approach. Remote Sens. Environ. 155, 89–108. https://doi.org/10.1016/j.rse.2013.08.051.

Foreman, R.E., 1975. KIM-1: a method for inventory of floating kelps and its application to selected areas of kelp license area 12. In: Federal Fisheries and Marine Service and B.C. Marine Resources Branch, pp. 1–81.

Foster, M.S., Schiel, D.R., 2010. Loss of predators and the collapse of southern California kelp forests (?): alternatives, explanations and generalizations. J. Exp. Mar. Biol. Ecol. 393, 59–70. https://doi.org/10.1016/j.jembe.2010.07.002.

Fretwell, C., Boyer, L., 2010. Guidelines and methods for mapping and monitoring kelp forest habitat in British Columbia. Guidelines and methods for mapping and monitoring kelp forest habitat in BC. Mayne island conservancy society. Seagrass Conservation Working Group 1–13. https://seachangesociety.com/wp-content/uploads/2015/10/Kelp-Monitoring-Methods.pdf.
Fyfe, J.E., Israel, S.A., Chong, A., Ismail, N., Hurd, C.L., Probert, K., 1999. Mapping marine habitats in otago, southern New Zealand. Geocarto Int. 14, 17–28. https://doi.org/10.1080/10106049908542113.
Garcia, R.A., Fearns, P., Keesing, J.K., Liu, D., 2013. Quantification of floating macroalgae blooms using the scaled algae index. J. Geophys. Res. Ocean. 118, 26–42. https://doi.org/10.1029/2012JC008292.
Goldberg, S., Kirby, J., Licht, S., 2016. Applications of Aerial Multi-Spectral Imagery for Algal Bloom Monitoring in Rhode Island. SURFO Technical Report No. 16-01. http://digitalcommons.uri.edu/surfo_tech_reports/13.
Gower, J., Hu, C., Borstad, G., King, S., 2006. Ocean color satellites show extensive lines of floating Sargassum in the gulf of Mexico. IEEE Trans. Geosci. Remote Sens. 44, 3619–3625. https://doi.org/10.1109/TGRS.2006.882258.
Gower, J., King, S., 2008. Satellite images show the movement of floating Sargassum in the gulf of Mexico and atlantic ocean. Nat. Preced 1–13 https://doi.org/10101/npre.2008.1894.1.
Gupta, R.P., Reet, T.K., Saini, V., Srivastava, N., 2013. A simplified approach for interpreting principal component images. Adv. Rem. Sens. 2, 111–119. https://doi.org/10.4236/ars.2013.22015.
Halpern, B.S., Cottenie, K., Broitman, B.R., 2006. Strong top-down control in southern California kelp forest ecosystems. Science (80) 312, 1230–1232. https://doi.org/10.1126/science.1128613.
Hardin, P.J., Jensen, R.R., 2011. Small-scale unmanned aerial vehicles in environmental remote sensing: challenges and opportunities. GIScience Remote Sens. 48, 99–111. https://doi.org/10.2747/1548-1603.48.1.99.
Hedley, J.D., Harborne, A.R., Mumby, P.J., 2005. Simple and robust removal of sun glint for mapping shallow-water benthos. Int. J. Remote Sens. 26, 2107–2112. https://doi.org/10.1080/01431160500034086.
Hernández, C.A., Sangil, C., Fanai, A., Hernández, J.C., 2018. Macroalgal response to a warmer ocean with higher CO2 concentration. Mar. Environ. Res. 136, 99–105. https://doi.org/10.1016/J.MARENVRES.2018.01.010.
Hogland, J., Billor, N., Anderson, N., 2017. Comparison of standard maximum likelihood classification and polytomous logistic regression used in remote sensing. Eur. J. Remote Sens. 46, 623–640. https://doi.org/10.5721/EuJRS20134637.
Hu, C., 2009. A novel ocean color index to detect floating algae in the global oceans. Remote Sens. Environ. 113, 2118–2129. https://doi.org/10.1016/j.rse.2009.05.012.
Hu, C., Feng, L., Hardy, R.F., Hochberg, E.J., 2015. Spectral and spatial requirements of remote measurements of pelagic Sargassum macroalgae. Remote Sens. Environ. 167, 229–246. https://doi.org/10.1016/j.rse.2015.05.022.
Huete, A.R., Justice, C., Van Leeuwen, W., 1999. MODIS Vegetation Index (MOD 13). EOS MODIS Algorithm-Theoretical Basis Document. NASA Goddard Space Flight Center, Greenbelt, Maryland.
Jensen, J.R., 2005. Introductory Digital Image Processing: a Remote Sensing Perspective, 3rd Ed. Pearson. Prentice Hall, Upper Saddle River, N.J.
Jensen, J.R., Estes, J.E., Tinney, L., 1980. Remote sensing techniques for kelp surveys. Photogramm. Eng. Rem. Sens. 46, 743–755.
Kay, S., Hedley, J.D., Lavender, S., 2009. Sun glint correction of high and low spatial resolution images of aquatic scenes: a review of methods for visible and near-infrared wavelengths. Rem. Sens. 1, 697–730. https://doi.org/10.3390/rs1040697.
Keesing, J.K., Liu, D., Fearns, P., Garcia, R.A., 2011. Inter- and intra-annual patterns of Ulva prolifera green tides in the Yellow Sea during 2007-2009, their origin and relationship to the expansion of coastal seaweed aquaculture in China. Mar. Pollut. Bull. 62, 1169–1182. https://doi.org/10.1016/j.marpolbul.2011.03.040.
Kim, A.M., Olsen, R.C., Lee, K., Jablonski, D., 2010. Using panchromatic imagery in place of multispectral imagery for kelp detection in water. Proc. SPIE Ocean Sens. Monit. II 7678, 12. https://doi.org/10.1117/12.850352.
Kislik, C., Dronova, I., Kelly, M., 2018. UAVs in support of algal bloom research: a review of current applications and future opportunities. Drones 2, 35. https://doi.org/10.3390/drones2040035.
Kotta, J., Remm, K., Vahtmäe, E., Kutser, T., Orav-Kotta, H., 2014. In-air spectral signatures of the Baltic Sea macrophytes and their statistical separability. J. Appl. Remote Sens. 8, 83634–83748. https://doi.org/10.1117/1.JRS.8.083634.
Krumhansl, K.A., Okamoto, D.K., Rassweiler, A., Novak, M., Bolton, J.J., Cavanaugh, K.C., Connell, S.D., Johnson, C.R., Konar, B., Ling, S.D., Micheli, F., Norderhaug, K.M., Pérez-Matus, A., Sousa-Pinto, I., Reed, D.C., Salomon, A.K., Shears, N.T., Wernberg, T., Anderson, R.J., Barrett, N.S., Buschmann, A.H., Carr, M.H., Caselle, J.E., Derrien-Courtel, S., Edgar, G.J., Edwards, M., Estes, J.A., Goodwin, C., Kenner, M.C., Kushner, D.J., Moy, F.E., Nunn, J., Steneck, R.S., Vásquez, J., Watson, J., Witman, J.D., Byrnes, J.E.K., 2016. Global patterns of kelp forest change over the past half-century. Proc. Natl. Acad. Sci. U. S. A 113, 13785–13790. https://doi.org/10.1073/pnas.1606102113.
Liew, O., Chong, P., Li, B., Asundi, A., 2008. Signature optical cues: emerging technologies for monitoring plant health. Sensors 8, 3205–3239. https://doi.org/10.3390/s8053205.
Ling, S.D., Johnson, C.R., Frusher, S.D., Ridgway, K.R., 2009. Overfishing reduces resilience of kelp beds to climate-driven catastrophic phase shift. Proc. Natl. Acad. Sci. 106, 22341–22345. https://doi.org/10.1073/pnas.0907529106.
Ma, L., Li, Y., Lan, G., Li, C., 2009. Large-sized seaweed monitoring based on MODIS. Proc. SPIE 7498, 749824–774826. https://doi.org/10.1117/12.832916.
Marmorino, G.O., Miller, W.D., Smith, G.B., Bowles, J.H., 2011. Airborne imagery of a disintegrating Sargassum drift line. Deep. Res. Part I Oceanogr. Res. Pap. 58, 316–321. https://doi.org/10.1016/j.dsr.2011.01.001.
Matthew, M.W., Adler-Golden, S.M., Berk, A., Richtsmeier, S.C., Levine, R.Y., Bernstein, L.S., Acharya, P.K., Anderson, G.P., Felde, G.W., Hoke, M.L., Ratkowski, A. J., Burke, H.K., Kaiser, R.D., Miller, D.P., 2000. Status of atmospheric correction using a MODTRAN4-based algorithm. In: SPIE Proceeding, Algorthims Multispectral , Ultraspectral Imag. VI 199–207. https://doi.org/10.1117/12.410341.
McCoy, R.M., 2005. Field Methods in Remote Sensing, first ed. Guilford Press, New York.
Mobley, C., 1994. Light and Water: Radiative Transfer in Natural Waters Inverse Methods for Estimating Inherent Optical Properties from Radiometric Measurements. Academic, San Diego, Califorina.
Mumford, T.F., 2007. Kelp and Eelgrass in Puget Sound. Puget Sound Nearshore Partnership Report No. 2007-05. U.S. Army Corps of Engineers. Seattle, Washington.
Murfitt, S.L., Allan, B.M., Bellgrove, A., Rattray, A., Young, M.A., Ierodiaconou, D., 2017. Applications of unmanned aerial vehicles in intertidal reef monitoring. Sci. Rep. 7. https://doi.org/10.1038/s41598-017-10818-9.
Nahirnick, N.K., Reshitnyk, L., Campbell, M., Hessing-Lewis, M., Costa, M., Yakimishyn, J., Lee, L., 2018. Mapping with confidence; delineating seagrass habitats using Unoccupied Aerial Systems (UAS). Remote Sens. Ecol. Conserv. 1–15. https://doi.org/10.1002/rse2.98.
Nezlin, N.P., Kamer, K., Stein, E.D., 2007. Application of color infrared aerial photography to assess macroalgal distribution in an eutrophic estuary, Upper Newport Bay, California. Estuar. Coasts 30, 855–868. https://doi.org/10.1007/BF02841339.
Nijland, W., Reshitnyk, L., Rubidge, E., 2019. Satellite remote sensing of canopy-forming kelp on a complex coastline: a novel procedure using the Landsat image archive. Remote Sens. Environ. 220, 41–50. https://doi.org/10.1016/j.rse.2018.10.032.
North, W.J., James, D.E., Jones, L.G., 1993. History of kelp beds (Macrocystis) in orange and san diego counties, California. Hydrobiologia 260–261, 277–283. https://doi.org/10.1007/BF00049029.
O'Neill, J.D., Costa, M., 2013. Mapping eelgrass (Zostera marina) in the Gulf Islands National Park Reserve of Canada using high spatial resolution satellite and airborne imagery. Remote Sens. Environ. 133, 152–167. https://doi.org/10.1016/j.rse.2013.02.010.
Pfister, C.A., Berry, H.D., Mumford, T., 2017. The dynamics of kelp forests in the northeast pacific ocean and the relationship with environmental drivers. J. Ecol. 1–14. https://doi.org/10.1111/1365-2745.12908.

Reed, D.C., Rassweiler, A., Carr, M.H., Cavanaugh, K.C., Malone, D.P., Siegel, D.A., 2011. Wave disturbance overwhelms top-down and bottom-up control of primary production in California kelp forests. Ecology 92, 2108–2116. https://doi.org/10.1890/11-0377.1.
Richards, G., Congalton, R.G., 2001. Accuracy assessment and validation of remotely sensed and other spatial information. Int. J. Wildland Fire 10, 321–328. https://doi.org/10.1071/WF01031.
Richards, J.A., 2013. Remote Sensing Digital Image Analysis: an Introduction, Remote Sensing Digital Image Analysis: an Introduction. Springer Berlin Heidelberg, Berlin, Heidelberg, Heidelberg. https://doi.org/10.1007/978-3-642-30062-2.
Roesler, C.S., Perry, M.J., 1995. In situ phytoplankton absorption, fluorescence emission, and particulate backscattering spectra determined from reflectance. J. Geophys. Res. 100, 279–294. https://doi.org/10.1029/95JC00455.
Rouse, J., Haas, R., Schell, J., Deering, D., 1974. Monitoring Vegetation Systems in the Great Plains with ERTS. Washington, DC. https://doi.org/10.1002/mrm.26868.
Schiel, D.R., Steinbeck, J.R., Foster, M.S., 2004. Ten years of induced ocean warming causes comprehensive changes in marine benthic communities. Ecology 85, 1833–1839. https://doi.org/10.1890/03-3107.
Schowengerdt, R.A., 2012. Remote Sensing Models and Methods for Image Processing, third ed. Academic Press, San Diego.
Shi, W., Wang, M., 2009. Green macroalgae blooms in the Yellow Sea during the spring and summer of 2008. J. Geophys. Res. 114, C12010. https://doi.org/10.1029/2009JC005513.
Son, Y.B., Min, J.-E.E., Ryu, J.-H.H., 2012. Detecting massive green algae (Ulva prolifera) blooms in the Yellow Sea and east China sea using geostationary ocean color imager (GOCI) data. Ocean Sci. J. 47, 359–375. https://doi.org/10.1007/s12601-012-0034-2.
Springer, Y., Hays, C., Carr, M., Mackey, M., 2007. Ecology and Management of the Bull Kelp, Nereocystis Luetkeana: A Synthesis with Recommendations for Future Research. Lenfest Ocean Program, Washington, D.C., USA.
Stekoll, M.S., Deysher, L.E., Hess, M., 2006. A remote sensing approach to estimating harvestable kelp biomass. J. Appl. Phycol. 18, 323–334. https://doi.org/10.1007/s10811-006-9029-7.
Sutherland, I.R., Karpouzi, V., Mamoser, M., Carswell, B., 2008. Kelp Inventory, 2007: Areas of the British Columbia Central Coast from Hakai Passage to the Bardswell Group. Ministry of Environment, Oceans and Marine Fisheries Branch.
Swain, P.H., King, R.C., 1973. Two Effective Feature Selection Criteria for Multispectral Remote Sensing. Laboratory for Applications of Remote Sensing (LARS) Technical Reports.
Taylor, D.I., Schiel, D.R., Taylor, D.I., Schiel, D.R., 2018. Algal populations controlled by fish herbivory across a wave exposure gradient on southern temperate shores. Ecology 91, 201–211.
Teagle, H., Hawkins, S.J., Moore, P.J., Smale, D.A., 2017. The role of kelp species as biogenic habitat formers in coastal marine ecosystems. J. Exp. Mar. Biol. Ecol. 492, 81–98. https://doi.org/10.1016/j.jembe.2017.01.017.
Tou, J.T., Gonzalez, R.C., 1974. Pattern Recognition Principles. Addison-Wesley, Reading, Mass.
Trebilco, R., Dulvy, N.K., Stewart, H., Salomon, A.K., 2015. The role of habitat complexity in shaping the size structure of a temperate reef fish community. Mar. Ecol. Prog. Ser. 532, 197–211. https://doi.org/10.3354/meps11330.
Uhl, F., Oppelt, N., Bartsch, I., 2013. Spectral mixture of intertidal marine macroalgae around the island of Helgoland (Germany, North Sea). Aquat. Bot. 111, 112–124. https://doi.org/10.1016/j.aquabot.2013.06.001.
Van Wagenen, R.F., 2015. Washington Coastal Kelp Resources: Port Townsend to the Columbia River, Summer 2014. Final Report. Washington Department of Natural Resources, Olympia, WA.
Vergés, A., Doropoulos, C., Malcolm, H.A., Skye, M., Garcia-Pizá, M., Marzinelli, E.M., Campbell, A.H., Ballesteros, E., Hoey, A.S., Vila-Concejo, A., Bozec, Y.-M., Steinberg, P.D., 2016. Long-term empirical evidence of ocean warming leading to tropicalization of fish communities, increased herbivory, and loss of kelp. Proc. Natl. Acad. Sci. 113, 13791–13796. https://doi.org/10.1073/pnas.1610725113.
Volent, Z., Johnsen, G., Sigernes, F., 2007. Kelp forest mapping by use of airborne hyperspectral imager. J. Appl. Remote Sens. 1, 011503. https://doi.org/10.1117/1.2822611.
Wang, M., Hu, C., 2016. Mapping and quantifying Sargassum distribution and coverage in the Central West Atlantic using MODIS observations. Remote Sens. Environ. 183, 350–367. https://doi.org/10.1016/j.rse.2016.04.019.
Wheeler, W.N., Smith, R.G., Srivastava, L.M., 1984. Seasonal photosynthetic performance of Nereocystis luetkeana. Can. J. Bot. 62, 664–670.
Yu, Q., Gong, P., Clinton, N., Biging, G., Kelly, M., Schirokauer, D., 2006. Object-based detailed vegetation classification with airborne high spatial resolution remote sensing imagery. Photogramm. Eng. Rem. Sens. 72, 799–811. https://doi.org/10.14358/PERS.72.7.799.